# DLR ANALYSIS ON THE NOISE EMISSION FROM THE RACER CONFIGURATION

Jianping Yin, Jianping.Yin@DLR.de, DLR (Germany), Thorsten Schwarz, Thorsten.Schwarz @DLR.de, DLR (Germany), Marc Wentrup, Marc.Wentrup@DLR.de, DLR (Germany), Frédéric Guntzer, Frederic.Guntzer@airbus.com, Airbus Helicopters (France)

**Abstract**
To answer the challenge of increasing range and speed of a rotorcraft, RACER (Rapid And Cost-Effective Rotorcraft) is developed by Airbus Helicopters. The RACER configuration incorporates an innovative “box-wing” design to provide lift and “pusher” propellers at the wing tips to generate thrust in forward flight. The noise sources from RACER do not only include conventional helicopter main rotor noise, but also propeller noise which can be significantly affected by interferences with the main rotor, wings and other parts of the configuration. Having been widely applied to the simulations of rotor and propellers, the DLR free wake code UPM and the aeroacoustic analysis tool APSIM are used for a detailed analysis and an improved understanding of the complex aerodynamics and aeroacoustics of the RACER configuration. The noise generation mechanisms of the various interactions among the propeller, the wings and the rotor as well as a variation in the sense of rotation of the propeller are numerically studied to allow finding mitigation means to reduce the interactions in the final RACER configuration. The noise from rotor and propeller emitted by the complete RACER configuration for various flight conditions is analyzed and the analysis of acoustic scattering of propeller noise by the RACER configuration is conducted.

## 1. INTRODUCTION

For traveling at cruise speeds around 400km/h (220kts), a high-speed demonstrator RACER (Rapid And Cost-Effective Rotorcraft) is developed by Airbus Helicopters within the CleanSky 2 European research program. The RACER design draws upon the expertise and competencies of 38 European partners from 13 European countries, amongst which are the core partners ONERA (France) and DLR (Germany). ONERA and DLR have joint their competencies to carry out activities [1] related to the aerodynamic and aeroacoustic design of RACER. The RACER configuration and the workshare between DLR and ONERA are illustrated in Figure 1. ONERA contributed to the design of the propellers, and the vertical fins (VF), whilst the acoustic analysis is being carried out jointly by DLR and ONERA. The DLR was in charge of the aerodynamic design of the wing, and of the horizontal stabilizer (HS). The wing is designated to share the lift generation with the main rotor (MR) to decrease its loading. Additionally two propellers or lateral rotors (LR) in pusher configuration are installed at the wing tips to relieve the main rotor from thrust generation in forward flight. Thus the main rotor is further unloaded, enabling faster and more efficient cruise flight. Due to its unique configuration, the noise sources from RACER do not only include conventional helicopter main rotor noise, but also propeller noise.

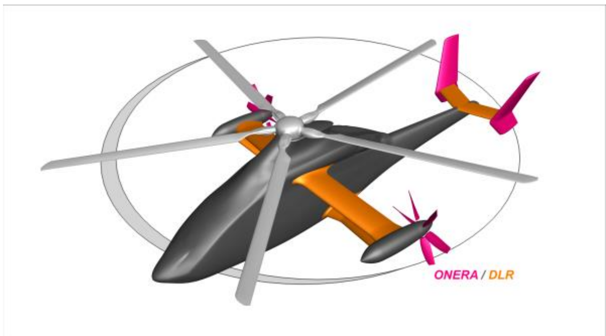


*Figure 1 illustration of DLR and ONERA workshare*

The activities presented in this paper are focused on DLR analysis on the noise emission from the RACER configuration. In particular the analysis of the noise generating mechanisms due to the interactions among the wings, the rotor and the propeller is addressed. The purpose of these studies is to allow predicting the interactions before they occur and therefore finding mitigation means in a pro-active way. The aerodynamic simulations necessary for the aeroacoustic predictions are conducted with the free wake panel method (UPM)[2][3], which is capable to simulate all aerodynamic interferences between the components of the full RACER configuration. The Ffowcs Williams-Hawkings (FW-H)-equation based code APSIM[4] is used to predict the acoustic emissions from the rotor and propellers. Finally, the acoustic scattering effects due to the fuselage and wings are studied using the DLR Boundary Element Method FMBEM[7].



Presented at 45th European Rotorcraft Forum, Warsaw, Poland, 17-20 September, 2019

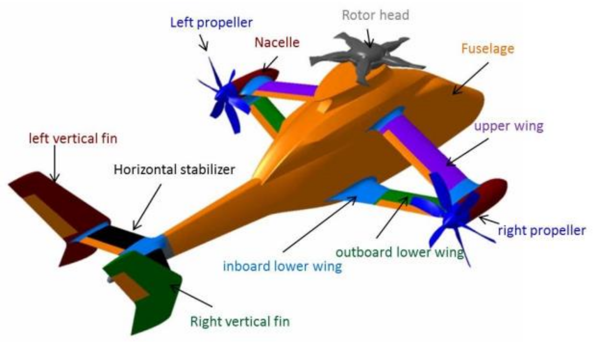


*Figure 2 The complete NACOR configuration including propellers*

## 2. RACER MODEL AND FLIGHT CONDITIONS

The RACER, as shown in Figure 1 and Figure 2 is a mid-weight helicopter with a staggered box wing and an H-shape empennage. The box wing section consists of an upper wing (UW) part which is connected by the nacelles at the tip with the lower wing part (LW). The propeller rotation direction was set to counter rotate with respect to the wing tip vortex direction, which means that the right propeller turns in clock wise direction (view from behind) and the left propeller rotates in counter clock wise direction (view from behind). Thus by taking advantage of the swirl recovery from the wing tip vortex, the propellers efficiency can be improved. The outer geometry of the RACER demonstrator was delivered by Airbus Helicopters (AH) to ONERA and DLR for acoustic evaluations. The flight conditions and the aircraft trim were computed by AH using the AH-In-house flight dynamic code HOST[5]. Two certification flights are presented in the following sections: the first one is level flight with 85m/s in which the propeller noise is important; the second one is the 6° descent flight with 46m/s in which main rotor BVI is dominant.

According to the trim condition provided by AH and considering rigid blade motions, the pitch angles of both propellers and of the main rotor (MR) were adjusted in the UPM computation to match the given thrust. The main rotor cyclic pitch and rigid flap angle is taken directly from the trim condition provided by AH.

## 3. DLR METHODOLOGIES APPLIED IN NUMERICAL SIMULATIONS

The numerical chain applied for the investigations is shown in Figure 3. The flight dynamics code HOST[5] provides the required trim condition for the aerodynamic simulations using UPM. The free-wake panel method UPM is based on a velocity-based, indirect potential formulation using a combination of source and vortex distribution on the solid surfaces and vortex panels in the wake. Compressibility effect of the flow is considered by applying the Prandtl-Glauert correction. The blade vortex interaction (BVI) is captured thanks to the free wake model used in UPM. Depending on the configurations, all interactions among propellers, rotor, fuselage, wings and tail are considered. By postprocessing the unsteady aerodynamic pressure on the blade surface, the Ffowcs Williams-Hawkings (FW-H)-equation based code APSIM is used to compute the noise radiation and to predict the acoustic levels on a given hemisphere surface. Finally, a Fast Multipole Boundary Element Method (FMBEM) code [7][8][9] is used for solving the scattered pressure field of the fuselage and wings and to access the impact of noise scattering on the propeller noise. The FMBEM code solves the exterior Helmholtz problem (scattering problem). It is a BEM method accelerated by the fast multipole method (FMM) for triangulated surfaces. The Burton-Miller approach is used to guarantee the uniqueness of the solutions. By giving the incident acoustic pressure, the solution (total acoustic pressure) can be derived from the Helmholtz Equation (using Green's function, solid wall and far field boundary condition).

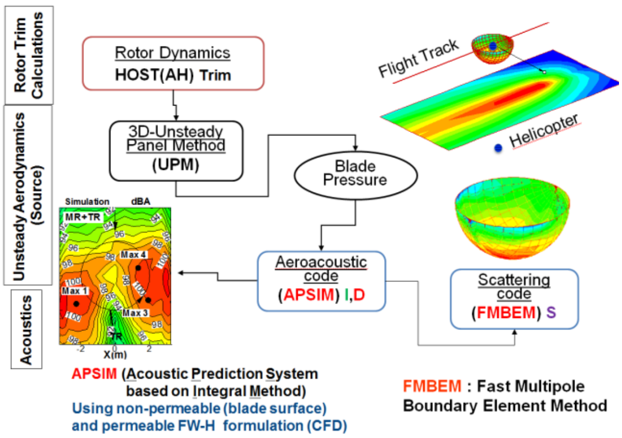


*Figure 3 the numerical chain for the simulations*

Validations of UPM and APSIM were intensively conducted during various projects. Detailed descriptions on the validation for the main rotor (MR) of a BO105 wind tunnel model in blade vortex interaction condition are given in [2][3][6].

## 4. PROPELLER-ROTOR-WING INTERACTION (WITHOUT ACOUSTIC SCATTERING)

To get a general understanding of the Propeller-Rotor-Wing interaction-noise generation mechanisms, different combinations of the components and their interactions are studied. The flight condition chosen is the certification



Presented at 45th European Rotorcraft Forum, Warsaw, Poland, 17-20 September, 2019

flyover condition at $V_0$=85 m/s where both the propeller and MR can radiate noise. At this place, only the right propeller and its corresponding wings without nacelle are taken into consideration (see Figure 4). The investigation of the propeller in two different rotational directions is also considered. The propeller thrust is trimmed to the same value in all simulations.

### 4.1. Propeller-Wing interaction

To determine the impact of the different wing parts on the pusher propeller noise emission, the following combinations are investigated at constant propeller thrust:

- Propeller+Upper Wing (UW)
- Propeller+Upper+Lower Wing (UW+LW)

In addition, a variation of the propeller thrust is also studied to understand the effect of the propeller thrust on the interaction noise. In the discussion of the aerodynamic interactions, the focus is placed on those aspects that are of primary relevance for the noise generation mechanisms, such as the characterization of the blade loading and its time gradients as function of propeller azimuthal position. Due to the inviscid flow modelling in UPM, the impact of the trailed boundary layer behind the wings is not considered.

The blade azimuthal position is defined according to a reference blade position for each propeller, the definition of which is shown in Figure 4. The initial position, the angle of φ = 0◦, is defined as corresponding to the reference blade pointing upwards along the z-axis. The blade reference angle increases in the direction of rotation i.e. count-clockwise for the propeller rotating with wing tip vortex (shown in blue in Figure 4, view from behind) and clockwise for the propeller rotating against wing tip vortex (shown in red, view from behind), when looking from upstream. The rotational direction of the wing tip vortex is defined according to positive wing lift. The acoustic characteristics are discussed based on acoustic assessments on 150m hemispheres.

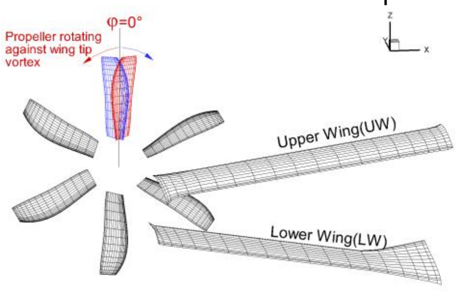


(a) perspective view

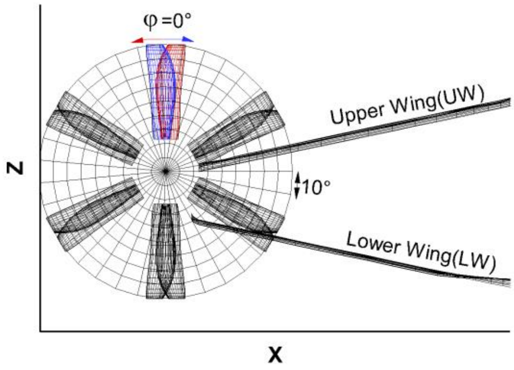


(b) front view

*Figure 4 Configuration and blade azimuthal angle definition used in propeller-wing studies, looking downstream, perspective(a) and front (b) view*

#### 4.1.1. Propeller+Upper Wing (UW)interaction

The effects of the wing on the propeller are mainly caused by the displacement of the wing potential field and the wing wakes, which vary over time due to the interactions with the potential field and the wake of the bypassing propeller blades. Figure 5 shows the wing induced velocity components within the propeller disk area (dashed circle), where Vy is the induced velocity (Figure 5b) in propeller axial y direction. The induced velocity fields indicate that there is a slight flow deceleration (negative value) in axial y-direction, especially in the area below the wing (represented by the black bar). The magnitude of the deceleration is relatively weak in comparison with in-plane components Vx and Vz. The wing creates a downwash while the tip-vortex causes an upwash beyond the wing tip as shown by the flow vectors in Figure 5b. When the propeller rotates counter clockwise against the wing tip vortex, this increases the Mach number due to the superposition of the induced velocity (mainly x-z components). Therefore, the propeller lift is increased when the propeller rotates towards the wing (from the lower part of the wing). The interaction between propeller and wing becomes strongest when the blade cuts through the wing wake at about 270°. These characteristics can be easily identified in the lift time histories of the propeller blade as a function of propeller revolution as shown in Figure 6. When the propeller rotates clockwise with the wing tip vortex, the effect of the interaction causes a reduction of the blade lift when the propeller rotates towards the wing (from the upper part of the wing).



Presented at 45th European Rotorcraft Forum, Warsaw, Poland, 17-20 September, 2019

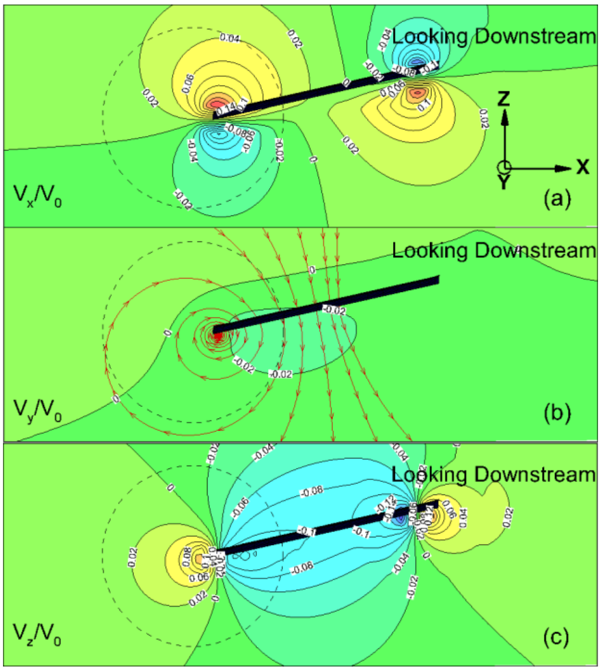


*Figure 5 Snapshot of the flowfield within the propeller disk area for the isolated up-wing*

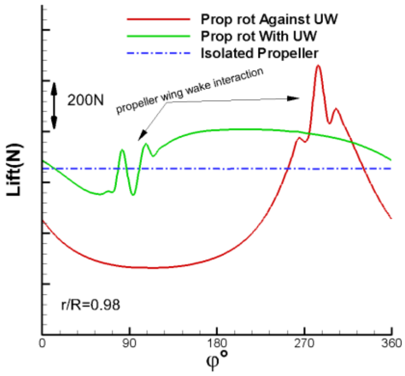


(a) Time history of blade lift at r/R=0.98

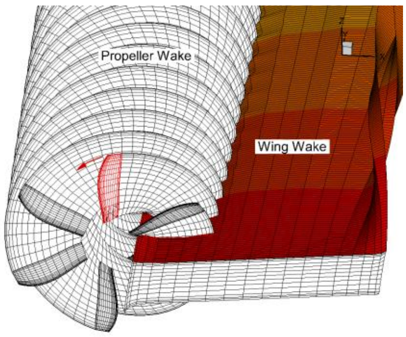


(b) Wake system of propeller and wing wake

*Figure 6 Blade lift time history and propeller and wing wake development*

A deeper analysis of the sectional load histories plotted in Figure 6a shows that interactions of the propeller with the wing potential field exhibit a smooth lift variation in one per revolution (1-P) behaviour (green line) and a stronger (1-P) variation when the propeller rotates against wing tip vortex (red line). As the propeller blade cuts through the wing wakes, as shown in Figure 6b, direct blade-wing wake interactions occur. The direct blade-wake interactions display a sudden change in the lift time history (BVI behaviour) as marked by the arrow in Figure 6a. The interaction for the propeller rotating against the wing tip vortex (red line) is relatively stronger compared with the interaction for the propeller rotating with wing the tip vortex (green line), as illustrated in Figure 5

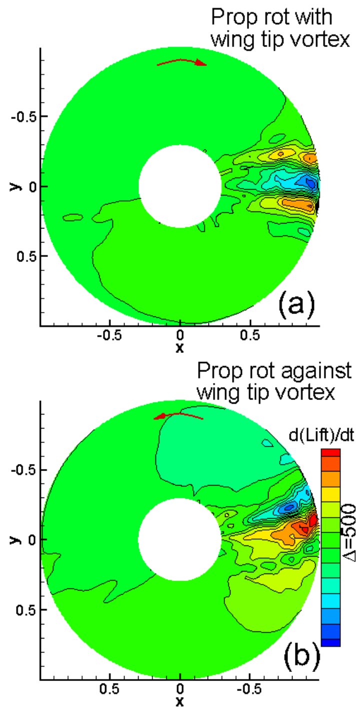


*Figure 7 Lift time gradient contours on the propeller disc for two different rotational directions (configuration propeller+UW)*

The strength and position of the unsteady noise sources caused by interactions can be visualized in terms of lift time gradient contours on the propeller disc, as shown in Figure 7 for the two different rotational directions. The comparison indicates that the variations of the propeller lift occur around azimuthal positions at the right side of the disc where the wing is located. The variations extend from blade tip to the root in this area. The wing wake causes a sudden change of the blades angle of attack which in combination of the rising stagnation pressure towards the blade tip results in a maximum lift change at the outer radius of the propeller. For the propeller counter rotating to the wing tip vortex, the wing wake affects an increase of the blade angle of attack and consequently increases the blade load.

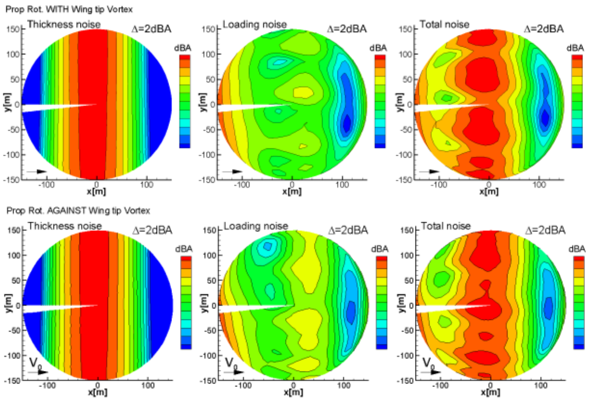


*Figure 8 Noise contours in A-OSPL on 150m hemisphere underneath the propeller above and below: propeller rotating respectively against and with wing tip vortex*

Acoustic assessments of the propeller noise on 150m hemisphere underneath the propeller for the two different propeller rotational directions are shown in Figure 8. Due to the special orientation of the propeller, i.e. rotational plane directed towards the ground, it is interesting to divide noise from a propeller into its distinct sources, such as thickness noise (left) and loading noise (middle). The characteristics of the thickness noise indicates that thickness noise is primarily dominant in the plane of the rotation around x=0m and decays dramatically when the microphones move away from the rotational plane in up- and down-stream direction.

For the loading noise, the noise emission shows maximum in the area behind the propeller plane in slightly downstream direction, which is mainly from steady blade loading noise.

By comparing thickness noise with overall noise contours (right) as well as loading noise (middle), the maximum propeller noise is located around the rotational plane where thickness noise is dominant. In up- and down-stream direction the contribution mainly comes from the loading noise (middle) resulting from the unsteady load distribution.

When comparing loading noise for the two different rotational directions, slightly higher loading noise is observed for the propeller rotating with the wing tip vortex. This is consistent the with higher unsteady noise sources observed in Figure 7, bottom. In comparison with the thickness noise which has almost parallel contour lines, the contour lines of the total noise indicate some interference between the thickness- and the loading-noise around the propeller rotational plane, namely a cancelation between thickness- and loading-noise. In addition, as the blade in maximum noise source region is turning towards the sky if rotating against wing tip vortex (Figure 7 bottom), the Doppler amplification factor can also help in this case to reduce the noise radiation towards the ground. It is observed that the maximum noise level is not significantly modified by the interaction but the noise is mainly increased in the far up- and down-stream directions due of the increase of the high order harmonics load created by the wings-propeller interaction.

The interactions of the propeller (potential field and the wake) with the wing also cause variations in wing lift which in turn can have an influence on the propeller interaction noise. The influence of the propeller on the wing aerodynamics is a function of the propeller thrust. To check such influence, simulations with reduced propeller thrust (-8%) are conducted for both rotational directions of the propeller. The differences of the total A-weighted sound pressure level between the cases with reduced propeller thrust and reference thrust are shown in Figure 9. The change of the propeller thrust has only minor influence with maximum 0.6 dBA at the downstream area. This indicates that for a pusher configuration, the wing/propeller interaction is more important for noise emission than the propeller/wing interaction. As the steady loading noise is mainly located in the low frequency range, the contribution to A-weighted sound pressure level caused by the propeller thrust variation remains limited.

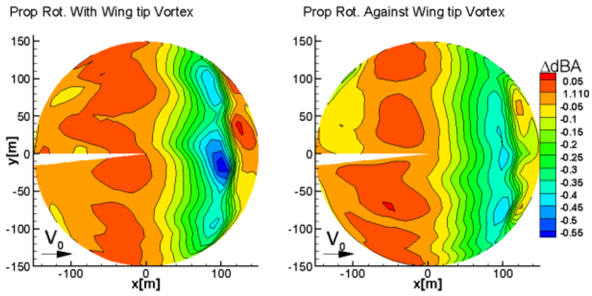


*Figure 9 the difference of the total A-weighted sound pressure level between reduced propeller thrust case and the reference thrust case*

### 4.1.2. Propeller+Upper Wing + Lower Wing (UW+ LW) interaction

Figure 10 shows the induced velocity components from both UW and LW within the propeller disk area (dashed circle). In comparison to Figure 5, the magnitude of the induced flow increases. Especially the maximum of the downwash flow in z-direction is extended to the inside of the propeller disk.



Presented at 45th European Rotorcraft Forum, Warsaw, Poland, 17-20 September, 2019

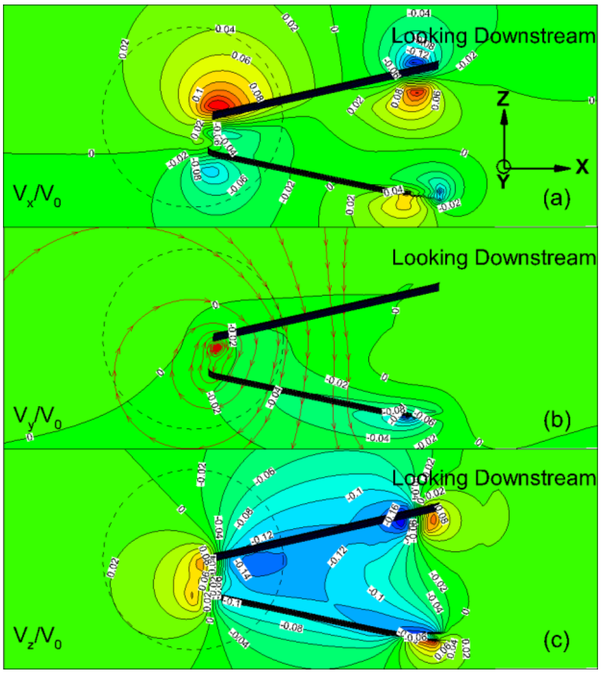


*Figure 10 Snapshot of the flowfield within the propeller disk area for the isolated up-wing and low-wing condition*

The propeller section lift at the blade tip region as function of one propeller revolution for the propeller+UW+LW configuration is given in Figure 11a and compared to the results from the propeller+UW configuration. Due to the addition of the LW, there are overall changes in the lift variation in the one per revolution (1-P) behaviour. The influence of the LW increases the dynamic loads of the propeller-UW interaction peaks, due to the increasing downwash indicated in Figure 10c and slightly shifts the azimuthal position of the propeller+UW interactions. This indicates a change in the UW wake system. The LW wakes also cut through the propeller rotational plane, as shown in Figure 11b. The additional peak values pointed by arrows in Figure 11a come from the blade-LW wake interaction, which are relatively weak compared with the propeller-UW interactions as the LW is less loaded.

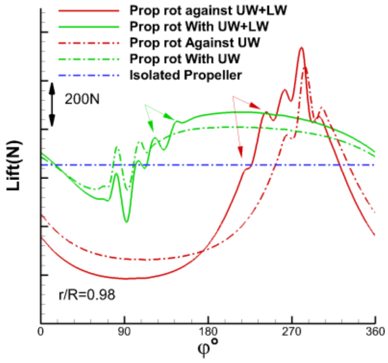


(a) Time history of blade lift at r/R=0.98

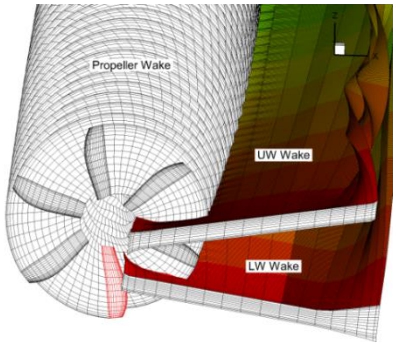


(b) Wake from propeller and UW+LW wake

*Figure 11 Blade lift time history and propeller and UW+LW wake development*

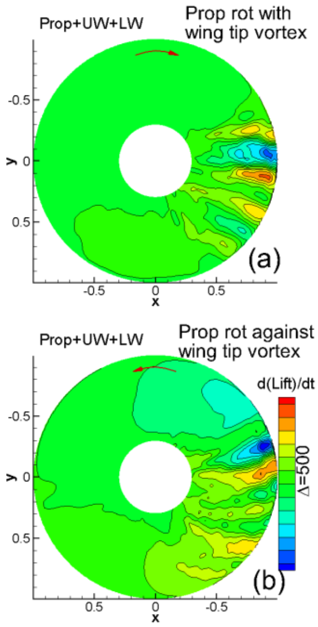


*Figure 12 Lift time gradient contours on the propeller disc for two different rotational directions (configuration propeller+UW+LW)*

The strength and position of the unsteady noise sources caused by interactions with UW and LW are shown in Figure 12 for the two different propeller rotational directions. The comparison with Figure 7 indicates that the unsteady noise sources extend to the area where propeller+LW interactions occur. In general, the strength of noise sources from the interactions with the LW is relatively weak in comparison with the interactions of the UW.



Presented at 45th European Rotorcraft Forum, Warsaw, Poland, 17-20 September, 2019

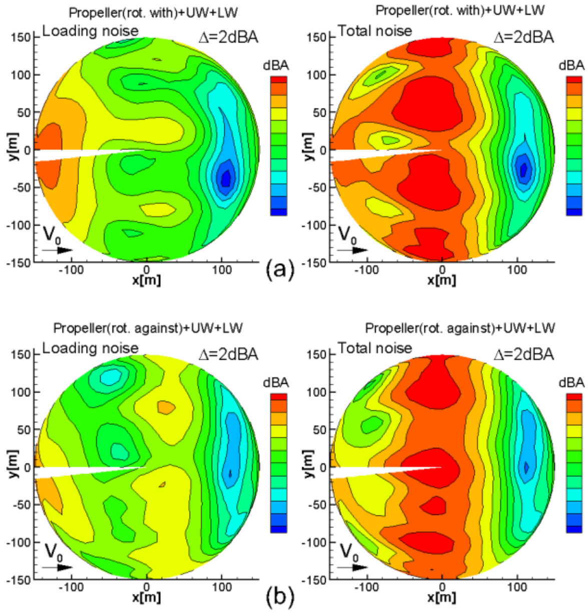


*Figure 13 Noise contours in A-OSPL on 150m hemisphere underneath the propeller, (a)Propeller rotating against wing tip vortex, (b) Propeller rotating with wing tip vortex*

The propeller noise on 150m hemispheres for the two different propeller rotational directions are shown in Figure 13. The thickness noise is almost the same as shown in Figure 8 as the same kinematic motion is applied. Therefore the thickness noise is not shown in Figure 13. The loading noise contains similar characteristics in terms of the noise directivity as demonstrated in Figure 8. Similar to the propeller+UW interaction case (Figure 8), the loading noise is dominant in forward (upstream) and rearward (downstream) direction due to the unsteady noise sources and the maximum total propeller noise is located around the rotational plane (thickness noise). In comparison with Figure 8, bottom, there is a slight reduction of the unsteady loading noise (Figure 13b) in upstream direction for the propeller rotating against the wing tip vortex, while the additional interaction from the LW causes an increase of the unsteady loading noise (Figure 13a) in upstream direction for the propeller rotating with the wing tip vortex. For this configuration, the propeller rotating against the wing tip vortex is 0.6dBA less noisy than that rotating with the wing tip vortex in terms of the maximum total noise level.

### 4.2 Propeller-Rotor interaction

The effects of the main rotor on the propellers and the propeller wake mainly come from the flow displacement (potential field) induced by the main rotor (MR) blades and MR wakes. Figure 14 illustrates a snapshot of the wake development for the Propeller+Rotor configuration where the propeller is rotating against the wing tip vortex. The snapshot shows that there is a clear distance between the MR wake and the propeller, which indicates that there is no direct interaction between the MR wake and the propeller. The characteristics of the wake development for the propeller rotating with the wing tip vortex are similar to the case shown in Figure 14.

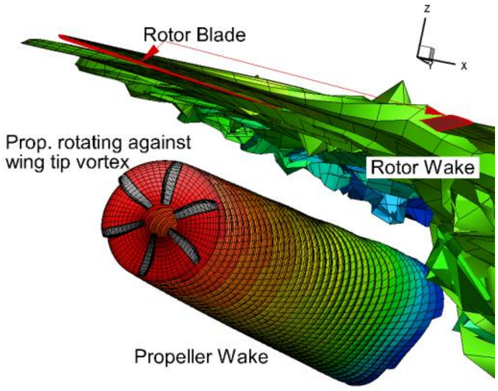


*Figure 14 Snapshot of wake development for the Propeller+Rotor configuration*

Figure 15 shows the MR induced velocity components within the propeller disk area (dashed circle). There is a relative large flow deceleration in axial y-direction, located at the MR advancing blade side. The magnitude of the deceleration is relatively weak in comparison with the x and y-components. The MR has created an upwash in the x-z plane at the MR retreating blade side area where the left propeller is located (dashed circle). Independent of the propeller rotational direction, the MR upwash increases the blade force of the propeller as the Mach number of the propeller in the first half of the revolution between 0 and 180° and becomes maximum around 90° is increased.

The propeller rotates about 6 times faster than the main rotor. This affects that the flow conditions for succeeding propeller revolutions differ due to the different relative locations of the main rotor blades and MR wakes. Figure 16 shows propeller lift time histories as a function of six consecutive propeller revolutions overlapping one MR revolution. The difference between the blue dashed line for the lift of an isolated propeller and the red or green solid lines demonstrate the influence of the rotor on the propeller lift while the difference among different solid lines represents the influence of the relative positions and motions between the rotor and the propeller. This influence is slightly larger for the propeller rotating with the wing tip vortex. In comparison with the isolated propeller case, an



Presented at 45th European Rotorcraft Forum, Warsaw, Poland, 17-20 September, 2019

increasing low frequency 1-P component is observed, indicating increasing asymmetry of the mean flow in the propeller plane. The positions of the maximum propeller blade force are located around 90° as explained in Figure 15. Comparing with the propeller-wing interactions, there are no blade wake interaction peaks because there is no direct MR wake / Propellers interaction as it can be seen in Figure 14.

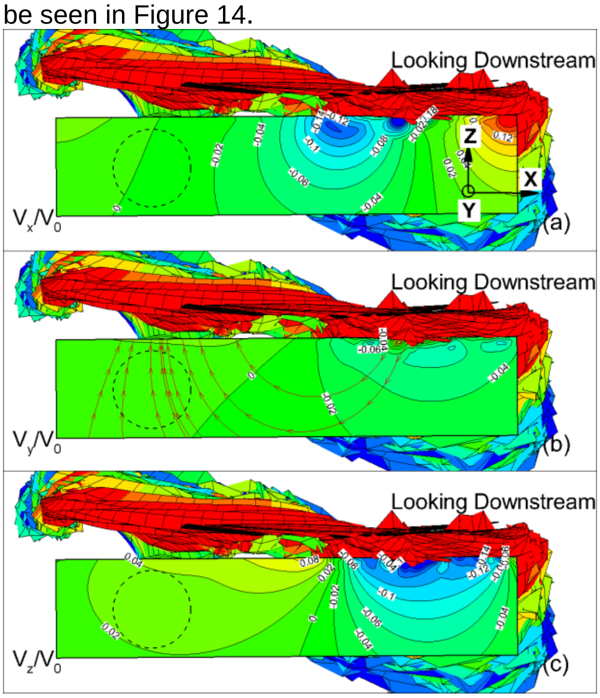


*Figure 15 Snapshot of the flowfield within the propeller disk area for the isolated MR condition*

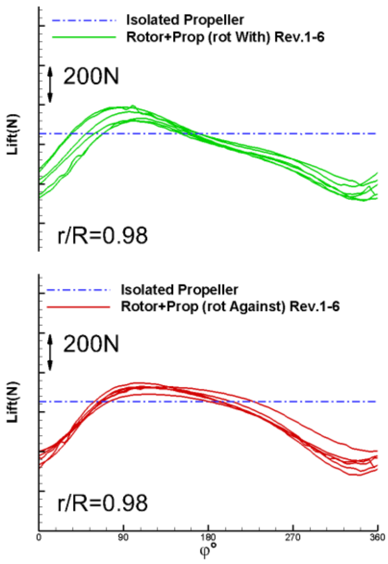


*Figure 16 Time history of blade lift at r/R=0.98 for 6 continue propeller revolutions*

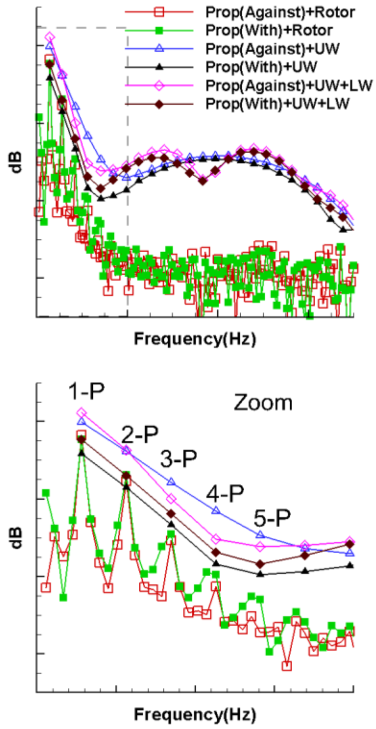


*Figure 17 Spectral analysis of propeller unsteady loadings at r/R=0.98 among varius configurations*

Figure 17 plots the spectral analysis of the lift time history for various configurations for the selected section at r/R=98. In general, the time history length of one propeller revolution is taken for the spectrum analysis except for the propeller-rotor configuration where the time history with 6 propeller revolution is used, therefore the spectrum resolution is higher compared with other configurations. In general, the propeller-wing(s) interactions result in higher spectrum values for the harmonics above 3-P due to the direct interaction between propeller blade and wing wake. The interference effects caused by the lower wing increase the interaction harmonics above 5-P. In the propeller-rotor configuration, the dominant source of the fluctuations is linked to the interaction of the rotor induced potential field. The largest amplitude fluctuation occurs at the first (1-P) and second (2-P) propeller rotational frequency. For the propeller rotating against the wing tip vortex the spectrum contains higher values in comparison with the case when the propeller is rotating with the wing tip vortex. The 1P-loading fluctuation represents the increased asymmetry of mean flow in propeller plane.



Presented at 45th European Rotorcraft Forum, Warsaw, Poland, 17-20 September, 2019

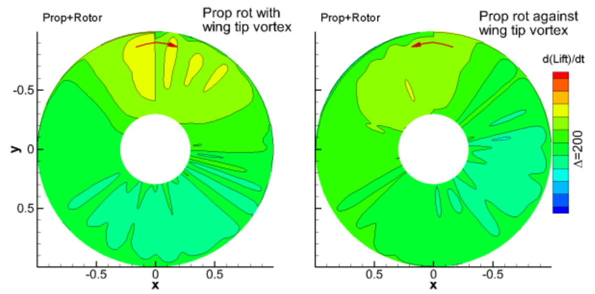


*Figure 18 Lift time gradient contours on the propeller disc for two different rotational directions (configuration propeller+Rotor)*

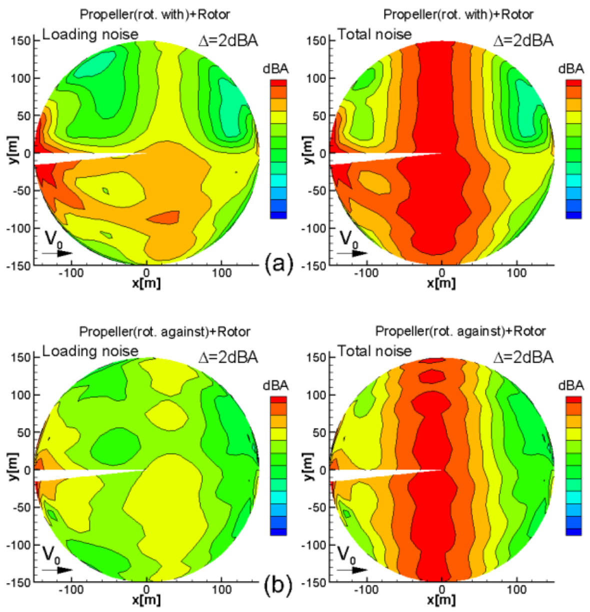


*Figure 19 Noise contours in A-OSPL on 150m hemisphere underneath the propeller, (a)Propeller rotating against wing tip vortex, (b) Propeller rotating with wing tip vortex*

The contour plots of the sectional lift derivative for the propeller-rotor configuration are shown in Figure 18 for the two different rotational directions of the propellers. The contour plots which indicate the propeller unsteady noise sources show a relative smooth lift variation everywhere except in the upper part of the disc where the interaction caused by the rotor potential field is strongest due to the closer proximity to the main rotor.

Acoustic assessments of the propeller noise on 150m hemispheres for the two different propeller rotational directions are shown in Figure 19. By comparing the overall noise contours (right) with the configurations described in previous sections, the similar behaviour in the area located near the rotational plane indicates an acoustic interference effect between thickness- and loading-noise. Additionally, there is increasing unsteady loading noise at the edge of the rotational plane. Furthermore, unsteady loading noise is reduced when changing the propeller sense of the rotation from rotating with the wing tip vortex to rotating against the wing tip vortex. This linked with the higher unsteady noise source displayed in Figure 18left.

### 4.3 Propeller+Rotor+ UW+LW interactions

In this section, the influence of the interactions between Propeller, MR and Wings on the propeller noise generation is studied. Figure 20 shows the induced velocity components within the propeller disk area (dashed circle) for MR+UW+LW. Due to the upwash generated by the MR, the angle of attack of the wing increases. Therefore, the flow decelerations in axial y-direction in the area below the wings as well as the strengths of the x-z velocity components are increased. Due to the superposition of the induced velocities from both the wings and the MR, the overall induced velocity shows overall downwash in x-z plane as shown in Figure 20b, which indicates that the influence of the wings plays a dominant role. Therefore similar interaction behavior as section 4.1.2 is expected.

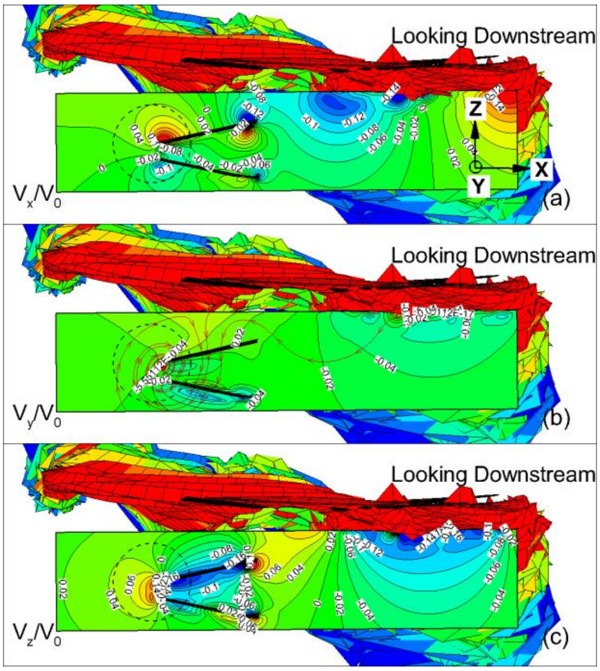


*Figure 20 Snnapshot of the flowfield within the propeller disk area for the MR+UW+LW condition*

Section lift at the propeller blade tip region as a function of one propeller revolution is given in Figure 21a and compared to the results of the propeller+UW+LW case. Due to the influence of both the rotor potential field and rotor downwash, there are overall changes of the propeller lift variation in one per revolution (1-P) behaviour.

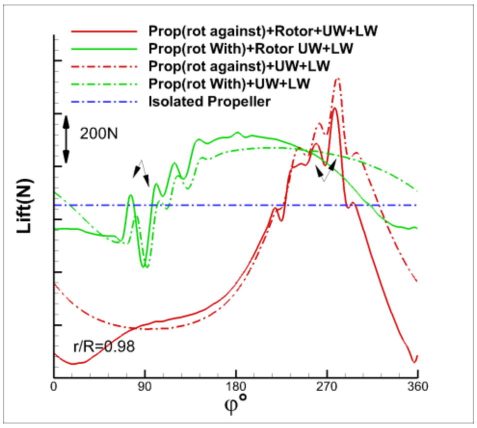


(a) Time history of blade lift at r/R=0.98

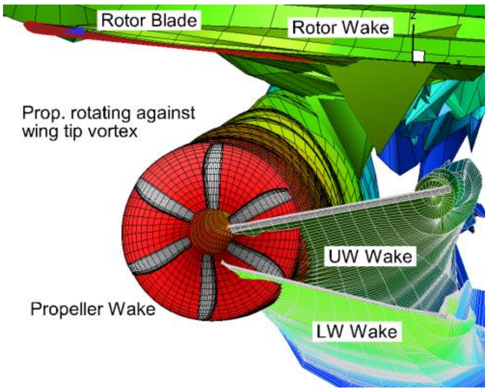


(b) Wake from propeller and UW+LW wake

*Figure 21 Blade lift time history and propeller and UW+LW wake development*

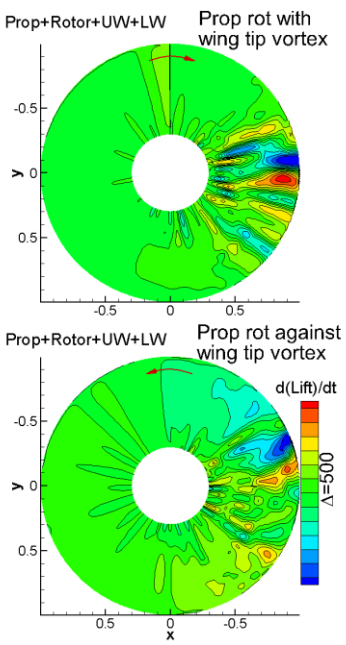


*Figure 22 Lift time gradient contours on the propeller disc for two different rotational directions (configuration propeller+rotor+UW+LW)*

Due to the interference effects the wing loading changes which in turn increase the dynamic load gradient of the propeller-UW interaction (indicated with arrow in the plot). There are no changes in the interaction positions between the propeller and the wings. Both the wakes from UW and LW cut directly through the propeller rotational plane, as shown in Figure 21b, but there is a clear distance between the MR wake and the propeller. This indicates that there are no direct MR wake/Propellers and MR wake/Wings interaction.

The contours of the propeller unsteady noise sources caused by interactions with the rotor, UW and LW are shown in Figure 22 for the two different rotational directions of the propeller. By comparing with Figure 12 and Figure 18, the interactions coming from the propeller with both UW+LW can still be easily identified. In general the strengths of the propeller-wing interactions increase for both rotational directions especially the interactions with the UW. This is due the rotor induced globally perturbed inflow, which is also indicated in the dynamic loads as shown in Figure 21a.

The influence of the rotor on the propeller-wings interaction noise can be derived by subtracting the noise from the propeller+UW+LW configuration, as shown in Figure 23. The positive values of A-weighted sound pressure level in the plot indicate an increasing propeller noise i.e. unsteady loading noise under the influence of the rotor. There is overall increasing noise in forward (upstream) and rearward (downstream) direction due to the increasing high frequency unsteady loading noise sources. It should be mentioned that high values in forward and rearward of hemisphere directivities are located in the high elevation angle region, and therefore are affected only by very long propagation paths and might have limited influence on ground due high atmosphere damping for long propagation distance. Figure 24 shows the comparison of the spectrum at two selected points marked in Figure 23. The comparison demonstrates that high spectrum value at frequencies above 3 Blade Passing Frequency (BPF) for both propeller rotational directions occur when taking into account the rotor effect. In addition, a slight increase of the unsteady loading noise is also observed in the propeller rotational plane, caused by changing blade 1-P loading. The propeller rotating with the wing tip vortex is much nosier when the main rotor is taken into account.

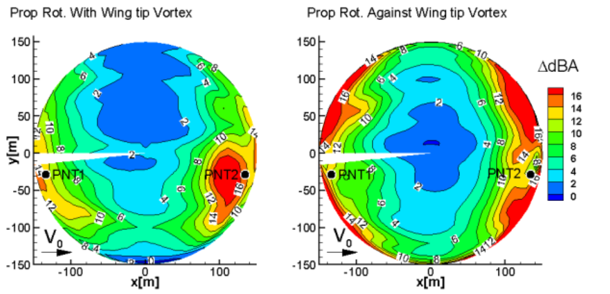


*Figure 23 the difference of the total A-weighted sound pressure level;influence of the rotor*

Therefore it should be noticed that the effect of the main rotor on the propeller-wing interaction cannot be neglected in the study of the propeller-wing interaction noise. The influence of the main rotor increases the levels of high harmonics of the propeller unsteady noise as well as overall noise level especially in up and down stream direction.

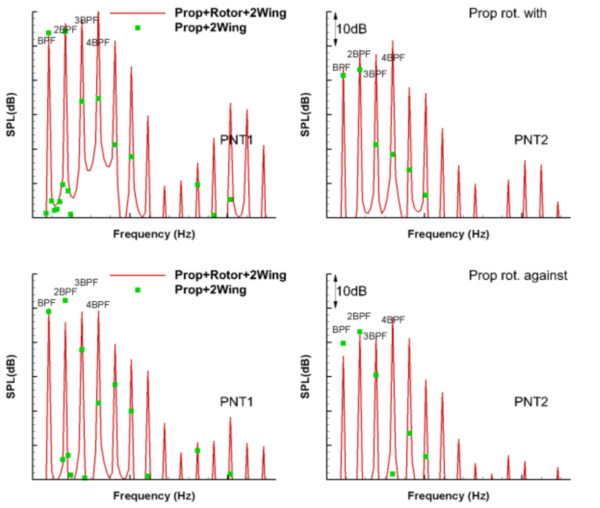


*Figure 24 SPL spectral analysis at PNT1 and PNT2 for two different propeller rotational direction*

### 4.4 Simulation of Complete Configuration

The aerodynamic and global acoustic evaluations from the complete RACER demonstrator, as shown in Figure 1, are discussed next. In this configuration, all interactions among propellers, main rotor, fuselage, wings and tail parts are considered. For RACER the propellers' rotation direction is set to counter rotate with respect to the wing tip vortex direction. The fuselage, tail boom, empennage and nacelle are modeled by a source/sink distribution on the surface. They are not considered as a lifting surface and thus contribute with zero net vorticity to the flow.

Two flight conditions are studied in this section, including (1) Certification level flight condition as used in the studies in previous sections; (2) Certification descent flight. For the first flight condition, the right propeller noise under complete configuration is compared with the case discussed in section 4.3 to investigate the influence of the airframe. In the second flight condition the main rotor blades are very close to their own wakes and cut through them; therefore there will be a higher focus on main rotor BVI.

#### 4.4.1 Certification level flight

The RACER configuration has two propellers, named right and left propeller defined when looking from behind to the upstream. The right propeller is the same as the propeller studied in the previous sections.

In order to compare with the results from section 4.3, the propeller nacelles are not included in the configuration for this flight.

In comparing the snapshot Figure 25 of wake development for the complete configuration with Figure 21, the following is observed:

- There is visually no obvious change in wing wakes in the area close to the right propeller except that the wing wake roll-up at the root region disappears due to the fuselage;
- There is no direct MR wake/Propellers interaction; the MR wake is much closer to the left propeller, therefore more influence is expected on the left propeller;
- The wing wake cuts through the propeller rotational plane causing direct blade-wake interactions.

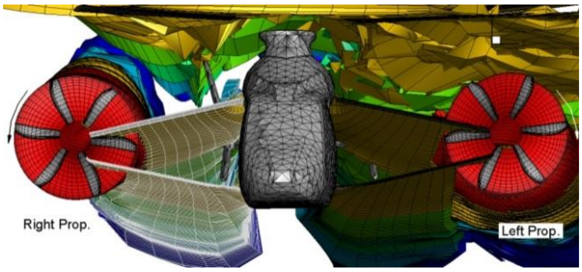


*Figure 25 Snapshot of wake development in level flight for the complete configuration*

Lift time gradient contours on right propeller disc and the time history at r/R=0.98 for the complete configuration are given in Figure 26. In terms of the propeller wing/rotor interactions, the characteristics of the contour pattern for the right propeller, as shown in Figure 26 top, is quite similar to Figure 22 bottom, except that the strengths of interactions is generally increased. Therefore higher levels of propeller noise are expected. By looking at the time history for r/R=0.98, a slight shift in the azimuth positions of



Presented at 45th European Rotorcraft Forum, Warsaw, Poland, 17-20 September, 2019

the interaction peaks is noticed, which indicates a change of the wing wake structure for the full configuration.

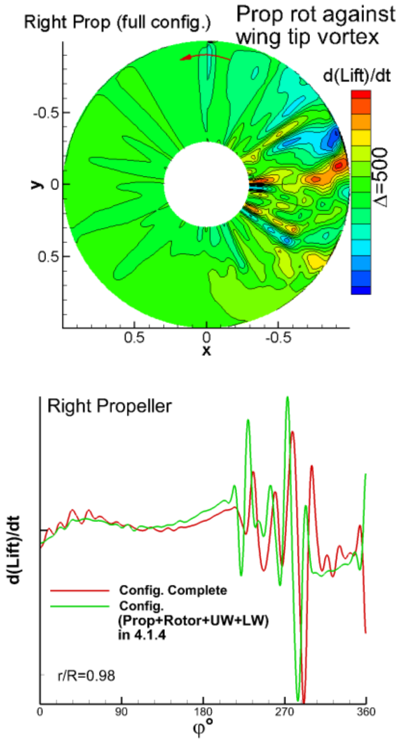


*Figure 26 Lift time gradient contours on right propeller disc and and time history at r/R=0.98 of the right propeller for full installed configuration*

By subtracting the right propeller noise computed for the propeller+rotor+UW+LW configuration from that of the full configuration, the influence of the additional components, such as fuselage, left propeller, etc. can be evaluated, as shown in Figure 27. The positive values of A-weighted sound pressure levels in the plot indicate an increase of the right propeller noise i.e. unsteady loading noise under full configuration. There is overall increasing noise in most of the hemisphere area, but a large reduction of the noise is observed at the edge area of the hemisphere for the full configuration. Therefore, when using right propeller noise simulated for a non-full-configuration, the flyover noise in the very far field will be overestimated, especially downstream of port side. Additionally the noise underneath the configuration will be underestimated.

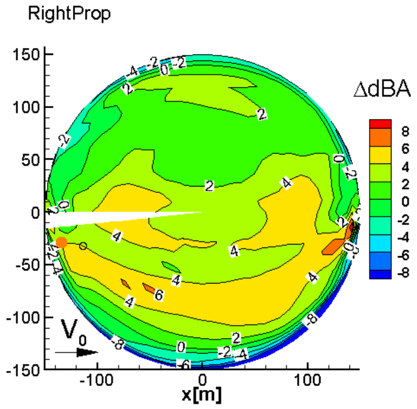


*Figure 27 the difference of the total A-weighted sound pressure level;influence of the fuselage and left propeller*

### 4.4.2 Certification descent flight

Snapshots of wake development for the certification decent flight condition in two different perspective views are given in Figure 28. For the clearness, only MR tip vortex trajectories are plotted in Figure 28b. The two propellers rotate in the direction against the wing tip vortex as marked by arrows. The wake development indicates that:

- The Rotor blades are very close to their own wakes and cut through them; therefore main rotor (MR) BVI is expected;
- There is a clear distance between MR wake and propellers, which indicates that there is no direct MR wake / Propeller interaction(Figure 28a); direct interactions between MR wake and propeller wake only occur in the propeller far wake region;
- The wing wake cuts through the propeller rotational plane which causes direct blade-wake interactions (Figure 28a) as explained in previous section;
- Direct interaction of the wing wake with tail parts is observed as shown in Figure 28b, which may cause tail parts lift variations as it was observed on the previous Airbus demonstrator X3.



Presented at 45th European Rotorcraft Forum, Warsaw, Poland, 17-20 September, 2019

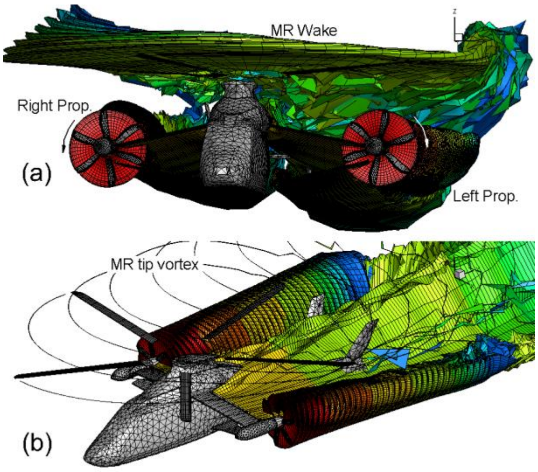


*Figure 28 Snapshots of wake development in descent flight for the complete configuration*

The unsteady noise source contours for both left and right propeller are shown in Figure 29. The characteristics of the contour pattern for the right propeller, as shown in Figure 29b, is quite similar to Figure 22(bottom), despite the two different flight conditions. The interactions coming from the propeller with both UW+LW as well as the influence of the main rotor can be identified. The interaction of the left propeller with UW+LW (Figure 29a) is much weaker than for the right propeller and therefore the left propeller is expected to be less noisy in this flight condition.

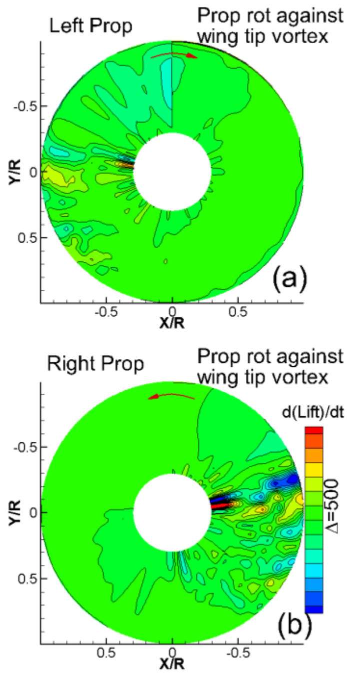


*Figure 29 Lift time gradient contours on the propeller disc for left(up)- and right(low)-propeller in complete configuration*

Acoustic assessments of the propeller noise on 150m hemisphere for the two propellers are shown in Figure 30. The right propeller exhibits higher unsteady loading noise especially in the upstream direction, while the unsteady loading noise for left propeller is stronger in the downstream direction (x>0). The right propeller is slightly less noise near the rotational plane as the results of a cancelation between thickness- and loading-noise.

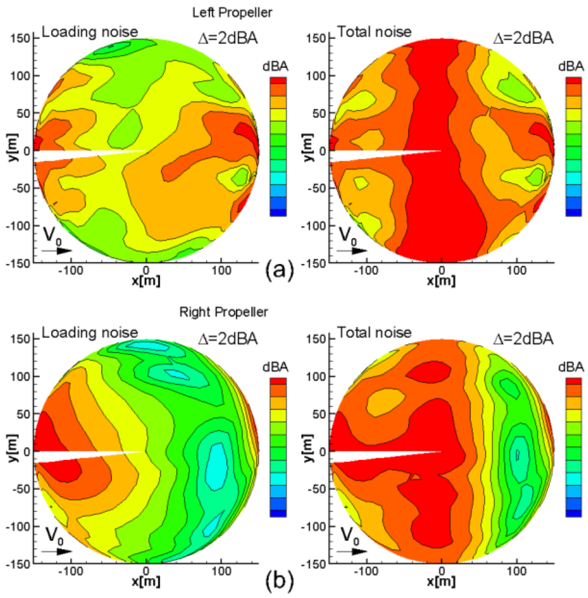


*Figure 30 Noise contours in A-OSPL on 150m hemisphere underneath the propeller, (a)Left Propeller, (b) Right Propeller*

MR lift time gradient contours as well as an example of the lift time gradient at r/R=0.98 for one revolution, are shown in Figure 31 for both isolated and installed MR. The characteristics of aerodynamic BVI at the advancing and retreating side of the full configuration are similar to that of the isolated rotor. The intense blade-parallel BVIs display as color bands in the contours and occur in the first and last quadrant of the disk as expected in this flight condition. The largest pressure fluctuations occur at the blade-parallel azimuth around 60° on the advancing side. On the retreating side, strong BVI is present at the tip around 348° as shown in time history at r/R=0.98. The installed configuration has increased MR BVI at both advancing and retreating blade due to aerodynamic displacement effects of the fuselage and wings. This additional perturbation field leads to increasing the noise.



Presented at 45th European Rotorcraft Forum, Warsaw, Poland, 17-20 September, 2019

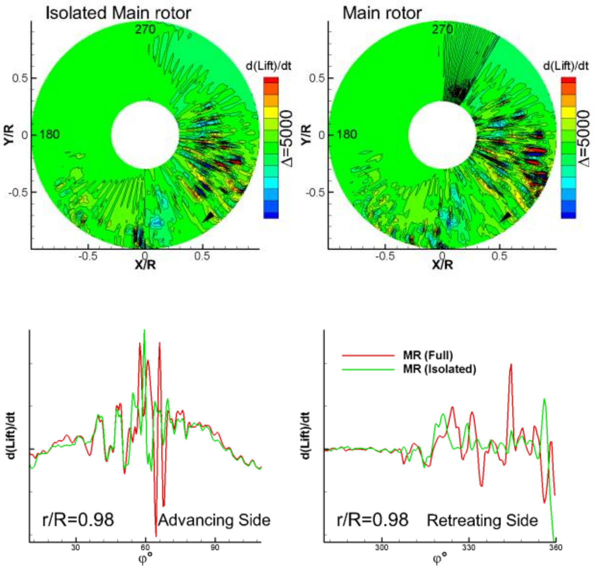


*Figure 31 Lift time gradient contours on rotor disc and and time history at r/R=0.98 for installed and isolated rotor*

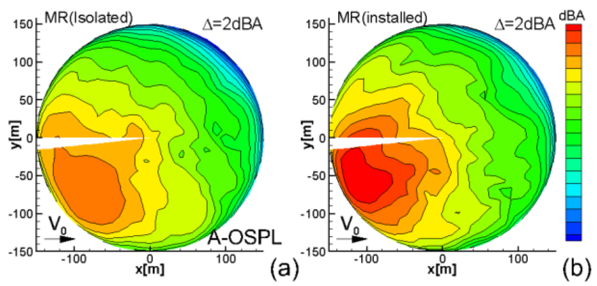


*Figure 32 Noise contours for the isolated and installed main rotor*

Acoustic assessments on 150m hemispheres for the main rotor noise of the isolated rotor and the complete configuration are shown in Figure 32. Similar rotor noise directivities for the full and the isolated configurations are observed. As expected from the analysis of the unsteady noise sources, an increase of the maximum levels by about 3.7dBA in noisier areas (hot spots) on the advancing side is visible for the complete configuration. This is also reflected in increasing BVI peak levels in Figure 31, especially in the outer part toward the blade tip. In this flight condition, unsteady loading (BVI) noise is dominant and the thickness noise is negligible.

The contour plot for the total noise of the propellers and rotor is illustrated in Figure 33. The characteristics of the contours indicate that:

- The maximum noise area reflects the characteristics of MR BVI noise (Figure 32 right);
- The contribution from the propeller noise is slightly seen near the propeller rotation plane.

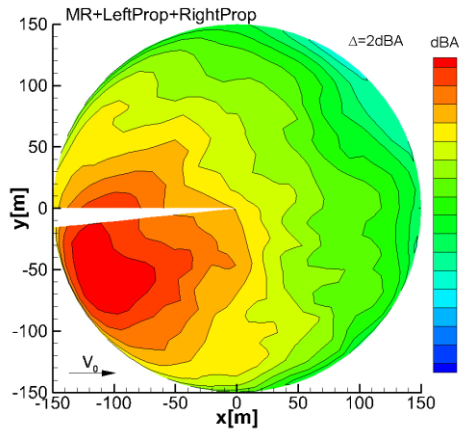


*Figure 33 Noise contours from sum of propellers+Rotor for the complete configuration*

## 5 ACOUSTIC SCATTERING EFFECT

The propeller noise scattering is addressed in this section. The propeller noise received by an observer in the far field is contributed by (1) the direct field (directly propagated from the noise source to the microphone) and (2) the scattered components from any obstacles, such as wings, as demonstrated in Figure 34. The scattered acoustic wave is an additional noise source which is a reaction of the wings to the acoustic incident wave. For the simplification on the analysis of the propeller noise under various interactions, only the direct field (1) was considered in previous sections and the wings or the fuselage scattering effect on propeller noise propagation was ignored.

In this section, the wings or fuselage scattering effect on propeller noise propagation is considered. The noise scattering effect (also called acoustic installation effect) by the wings is determined using a BEM (Boundary Element Method). For taking the scattering effect in the BEM computations into account, the propeller noise source is first propagated to a Kirchhoff source surface which encloses the propeller. This approach simplifies the modelling of the complex propeller noise source considerably. Figure 35 shows the cylindrical Kirchhoff surface used in propeller noise scattering predictions for the complete RACER configuration. The method of the source surface approach was used in the predictions of the rotor noise scattering as described in [9]. By prescribing the acoustic pressure and the normal derivatives of the incident field on the source surface, the scattering of the incident wave can be derived [7][9].



Presented at 45th European Rotorcraft Forum, Warsaw, Poland, 17-20 September, 2019

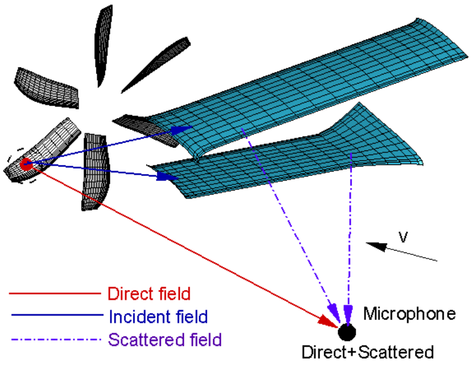


*Figure 34 Acoustic source component including scattered source*

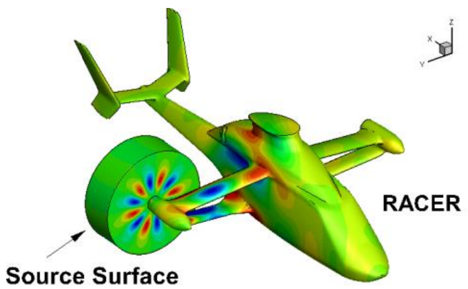


*Figure 35 Kirchhoff source surface for incident field of propeller noise*

To evaluate the influence of the scattering field, the shielding factor $\gamma$, defined as the ratio of total A-weighted pressure and total A-weighted incident pressure, is used.

$$\gamma = \frac{\sqrt{(\sum_{f=1}^{9} p_t^2(f))}}{\sqrt{(\sum_{f=1}^{9} p_i^2(f))}}$$

where the propeller harmonics from 1st to 9th BPF are summarized in A-Weighted form to get the shielding factor $\gamma$.

A shielding factor deviation from value 1 represents the effect of the scattering by the obstacles. The superposition of direct and scattered acoustic waves cause may cause noise canceling in “silent zones” or “shadow zones” ($\gamma < 1$) or an amplification of noise levels ($\gamma > 1$).

### 5.1 Acoustic scattering of the propeller noise by both right wings and full configuration

The impact of noise scattering is studied for the test case studies in section 4.3 where only the aerodynamic interactions among propeller, rotor and wings are taken into account. The configuration with the propeller rotating against the wing tip vortex is considered.

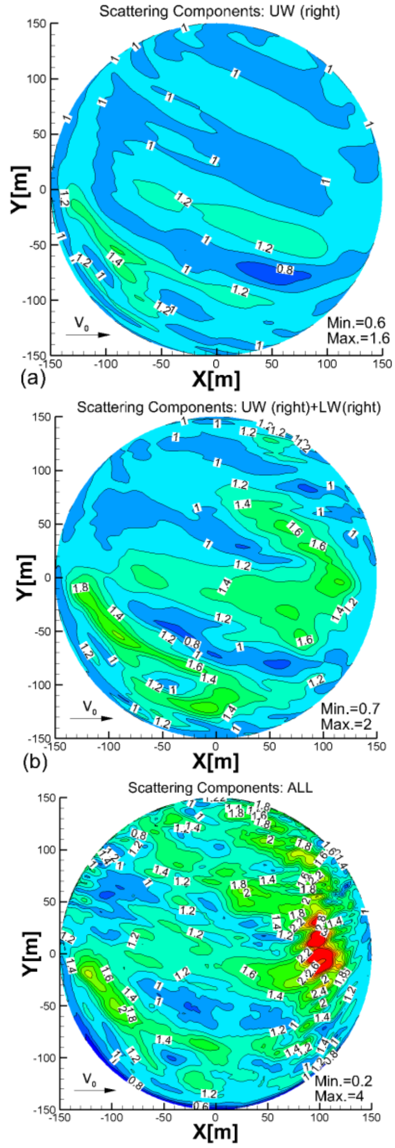


*Figure 36 Contour plot of shield factor for the scattering of both UW(upper) and UW+LW(lower); propeller source at propeller+rotor+UW+LW configuration*

Figure 36 shows the contour plot of the shielding factor on a 150m hemisphere as described before. The shielding factors for 3 different scattering components, namely UW(right), UW(right)+LW(right), and complete RACER, (see Figure 35), are compared.

In Figure 36, the general shielding characteristics can be observed by the shielding factor pattern. In general the more components are involved in the scattering; the more complicated are the scattering patterns. For example, adding the contribution of the acoustic scattering from the LW (right, Figure 36a) increases the deviation further from the value 1 and the complexity of the scattering pattern (Figure 36b). This indicates the importance to include the LW in the scattering simulation. The maximum deviation in the noise



Presented at 45th European Rotorcraft Forum, Warsaw, Poland, 17-20 September, 2019

emission considering the scattering effects from the UW and the UW+LW is from -2.0 to +2 dBA and from -1.5 to 3 dBA, respectively. When acoustic scattering from all components of the RACER is considered, as shown in Figure 36c, the deviation is further increased from -7.0 to +6 dBA.

## 6 CONCLUSION

The noise from rotor and propeller emitted by the complete RACER configuration for various flight conditions is analyzed as well as the acoustic scattering of propeller noise by the RACER configuration. All the NACOR calculations allow predicting the interactions before they occur and therefore finding mitigation means in the final configuration.

Thanks to it reduced peripheral velocity, propeller noise remains significantly lower than main rotor noise in the current analysis. As on a conventional helicopter, the main rotor remains the preponderant noise source on the RACER.

Yet the noise emission of the propeller can be significantly affected by interferences with the main rotor, wings and other parts of the configuration. Therefore the aerodynamic simulations required for the aeroacoustic predictions processed in frame of RACER noise evaluation include all aerodynamic interferences between the components of the full RACER configuration.

Following points can be drawn from the studies:

- Interactions of the propeller with the wing potential field exhibit a smooth lift variation in one per revolution (1-P) behaviour and are stronger when the propeller is rotating against the wing tip vortex;
- The direct blade-wing wake interactions displays a sudden change in the lift time history;
- Blade-wing wake interactions increase unsteady loading noise with a directivity in up- and down-stream direction, therefore highly damped by atmosphere due to long propagation paths;
- The effect of the main rotor on the propeller-wing interaction cannot be neglected in the study of the propeller-wing interaction noise as the influence of the main rotor increases the levels of the high harmonics of the propeller unsteady noise source;
- In descent flight BVI occurs in the analysed trim conditions, as for a conventional helicopter. Nevertheless on RACER, other trim conditions mitigating BVI noise can be considered as the compound architecture allows for it.
- Propeller noise in installed condition should be always evaluated as the scattering can change dramatic the noise directivity.

## 7 ACKNOWLEDGMENTS

The authors would like to thank the DLR core partner ONERA and the industrial leader Airbus Helicopters for the good, intense and fruitful cooperation. This project has received funding from the European Union’s Horizon 2020 research and innovation programme under grant agreement No CS2-AIR-GAM-2014-2015-01.

## 8 REFERENCES

[1] M. Wentrup, J. Yin, P. Kunze, T. Streit, J-H. Wendisch, T. Schwarz, J-P. Pinacho, K. Kicker, R. Fukari, “An overview of DLR compound rotorcraft aerodynamics and aeroacoustics activities within the CleanSky2 NACOR Project”. AHS Forum 2018. AHS Forum, 14-17.May 2018, Phoenix, Arizona

[2] J. Yin, B.G. van der Wall, G.A. Wilke “Rotor Aerodynamic and Noise under Influence of Elastic Blade Motion and Different Fuselage Modeling”. 40th European Rotorcraft Forum 2-5 September 2014, Southampton, UK.

[3] J. Yin, S.R Ahmed, “Helicopter main-rotor/tail-rotor interaction.” Journal of the American Helicopter Society, Vol. 45 (No. 4), Seiten 293-302, 2000

[4] J. Yin, and J. Delfs: Improvement of DLR Rotor Aeroacoustic Code (APSIM) and its Validation with Analytic Solution. 29th European Rotorcraft Forum, 2003

[5] B. Benoit, A.-M. Dequin, K. Kampa, W. von Gruenhagen, P.-M. Basset, and B. Gimonet: HOST, a General Helicopter Simulation Tool for Germany and France. 56th Annual Forum of the American Helicopters Society. Virginia Beach, VA, May 2-4 2000

[6] D. Rabe and G. Wilke: Parametric Design Studies of the Helicopter Rotor Noise using Variable-Fidelity Methods. AHS International 74th Annual Forum & Technology Display, 2018

[7] M. Lummer, C. Richtery, C. Pröber, J. Delfs, “Validation of a Model for Open Rotor Noise Predictions and Calculation of Shielding Effects using a Fast BEM”, 19th AIAA/CEAS Aeroacoustics Conference (34th AIAA Aeroacoustics Conference), 27 - 29 May 2013.

[8] J. Yin, K.-S. Rossignol, M. Barbarino, D. Bianco, C. Testa, H. Brouwer, S. Janssen, G. Reboul, L. Vigevano, G. Bernardini, M. Gennaretti, J. Serafini, C. Poggi, "Acoustical Methods and Experiments for Studying Rotorcraft Fuselage Scattering". 43rd European Rotorcraft Forum (ERF) 2017, 12-15 September 2017, Milan.

[9] J. Yin, "Investigation of Rotor Noise Shielding Effects by the Helicopter Fuselage in Forward Flight". Journal of Aircraft, Published Online: 21 Apr. 2019, The American Institute of Aeronautics and Astronautics (AIAA). DOI: 10.2514/1.C035009. ISSN 0021-8669.